Crystal Structure and Polymorphism of Poly(butylene-trans-1,4-cyclohexane dicarboxylate)

Crystal Structure and Polymorphism of Poly(butylene-trans-1,4-cyclohexane dicarboxylate)

Wenxian Hu[1,2]#, Tianyi Ma[1,2]#, Yong Zhou[1], Michelina Soccio[3], Nadia Lotti[3], Dario Cavallo[4], Dujin Wang[1,2], Guoming Liu[1,2]*

[1]Beijing National Laboratory for Molecular Sciences, CAS Key Laboratory of Engineering Plastics, CAS, Institute of Chemistry, Chinese Academy of Sciences, Beijing 100190, China

[2]University of Chinese Academy of Sciences, Beijing 100049, China

[3]Civil, Chemical, Environmental and Materials Engineering Department, University of Bologna, Bologna 40131, Italy

[4]Department of Chemistry and Industrial Chemistry, University of Genova, Genova 16146, Italy

# equal contribution

Corresponding author:

Guoming Liu: gmliu@iccas.ac.cn

For Table of Contents use Only

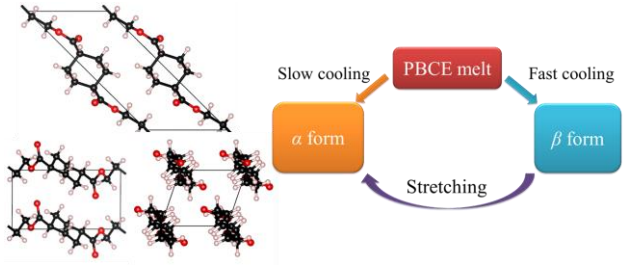

Abstract

The crystal structure analysis of a cycloaliphatic polyester, poly(butylene-trans-1,4-cyclohexane dicarboxylate) (PBCE), is carried out by X-ray fiber diffraction. Depending on the cooling condition, two crystal forms are identified (α and β). The α form is obtained by slow cooling from the melt, while the β form is generated during fast cooling. The α form has a triclinic unit cell with a $P\bar{1}$ space group, with parameters of a = 5.46 Å, b = 6.89 Å, c = 13.51 Å, α = 138.37°, β = 109.42°, γ = 63.30°. One PBCE chain is located in the unit cell with the chair conformation aliphatic rings and all trans- conformation methylene segmental parts. The structural transition and polymorphic transition during the heating and stretching process of PBCE are investigated by in-situ X-ray scattering. During heating, both the α and β forms show significant lattice distortion and eventually transform directly into the isotropic melt state. The volumetric thermal expansion coefficient of the PBCE α form was twice that of its unsaturated analog, poly (butylene terephthalate). On the other hand, the irreversible β-α transition occurs during stretching, indicating that the β form is a metastable phase.

1. Introduction

Bio-based polyesters, such as poly (lactic acid) (PLA), poly(ε-caprolactone) (PCL), poly(3-hydroxybutyrate) (PHB), etc., are of great significance for drug delivery, tissue engineering, packaging and coating,[1, 2] because of their biocompatibility and biodegradability. New biodegradable polyesters are being developed in academia and industry in seeking of better performance and lower cost.

Poly(butylene-trans-1,4-cyclohexane dicarboxylate) (PBCE), is a new kind of polyester. Cyclohexane units are included in the backbone, which enables the PBCE with good thermal stability, even higher than its aromatic polyester analog, poly (butylene terephthalate) (PBT).[3, 4] Compared with linear aliphatic polyesters, cyclohexane units also increase the stiffness of the chain. Thus PBCE has a relatively high melting temperature (~ 170 ºC).[4] On the other hand, because the aliphatic ring is more flexible than the benzene ring, PBCE has a lower glass transition temperature ($T_g \approx 20$ ºC) and higher impact resistance, as compared to PBT. Below T_g, PBCE has two secondary relaxations corresponding to the chain structure (aliphatic ring relaxation and $-(CH_2)_4-$ block relaxation).[3] The modulus and strength of PBCE are 830 MPa and 40 MPa, close to those of poly(l-lactic acid) PLLA,[5] which meets the requirements for food packaging, gas-barrier films, and plastics.[6] The possibility of applications in tissue engineering has also been explored.[4, 7-12] PBCE can copolymerize with other monomers, such as dimethyl diglycolate (DMDG), camphoric acid (CA), and bis(hydroxyl butylene) adipate (BHBA), providing versatile thermal and other physical properties.[4, 7, 8, 13]

PBCE is a highly crystalline polymer, as shown by X-ray diffraction. However, the crystal structure of PBCE has not been solved yet, which limits the deeper comprehension of the solid-state structure. The crystal structure, especially the chain conformation in the unit cell and interchain packing, is vital for understanding the physical properties of a polymer.[14, 15]

The crystal unit cell is the smallest structural element that possesses physical properties, including thermal, optical, electrical, and mechanical properties. Structure analysis of polymer crystals is most often carried out using uniaxial-oriented fiber diffraction.[16-23] Since the 1950s, with the development of new polyesters, the crystal structures of these polymers have been revealed.[24-33] Most of their unit cells belong to orthorhombic, e.g., poly(lactic acid) PLA β form, poly(ε-caprolactone) (PCL)[24], poly(glycolic acid) (PGA) α

form[25, 28], poly(3-hydroxybutyrate) (PHB) and poly(3-hydroxyvalerate) (PHV)[29] or monoclinic cells, such as poly(butylene succinate) (PBS)[27] and poly(butylene adipate) (PBA)[34]. Incorporating an aromatic ring in the backbone usually reduces the symmetry to triclinic, such as in poly (ethylene terephthalate) (PET),[26] PBT[35], and poly (butylene-2,6-naphthalate) (PBN).[36]

Since there are no reports on the crystal structure of polyesters that contain aliphatic rings, no direct reference is available for PBCE. The chemical structure of PBCE is most close to PBT, i.e., with a benzene ring replaced by a cyclohexane ring. Two crystal forms have been reported in PBT: α and β, both of which have triclinic unit cells.[35, 37] The conformation of α form in PBT is, TGGT$\bar{G}\bar{G}$T and the β form is TTTTTTT. The PBT chain in β form is more extended, as the β form is only stable under tension.[38] Another important issue in polyester is polymorphism. It was shown that PBCE exhibited different crystalline phases depending on the thermal and processing history, evidenced by X-ray diffraction.[8] However, the polymorphism and polymorphic transition has not been studied yet.

In this work, the crystal structure of the most stable form of PBCE (defined as the α form) was solved by X-ray fiber pattern. With fast cooling from the melt, a metastable crystal modification (defined as the β form) was preferentially formed. The β form transformed to the α form by stretching. An interesting feature of the PBCE α form is the high thermal expansion coefficient along the *a* and *b* direction, which may be a common feature in aliphatic ring-containing polymers.

2. Experimental section

2.1 Materials

PBCE was synthesized by condensation polymerization. Trans-1,4-cyclohexanedicarboxylic acid (CHDA) and 1,4-butanediol (BD) were used as feedstocks and the titanium tetrabutoxide, $Ti(OBu)_4$ (TBT), was employed as the catalyst. The synthesis procedure has been described in detail in the previous report.[9] Deuterated chloroform (containing 0.03% TMS) was purchased from Innochem.

2.2 Preparation of stretched sample of PBCE

The PBCE film with a thickness of ~ 200 μm was prepared by compression molding. First, the sample was melted at 220 °C for 1 min. Then, it was compressed at 220 °C under 50 MPa for 3 min. Finally, the film was transferred to a cold press for rapid solidification. The dumbbell-shaped specimens were cut from the middle of the film. The tensile bar was stretched with a rate of 25 μm/s at 100 °C to an engineering strain of 600 %, using a Linkam TST 350E hot stage. To increase the crystallinity, the stretched sample was annealed at 150 °C for 12 hours under the protection of inert gas. The slowly cooled sample was first heated to 220 °C, equilibrated for 3 min, and cooled to room temperature at about 4 °C/min.

2.3 Sample characterization

2.3.1 Gel permeation chromatography (GPC)

The molecular weight and molecular weight distribution of the samples were measured by GPC at 50°C using hexafluoroisopropanol (HFIP) as the solvent. A Waters e2695 equipment with a 2414 refractive index detector was used. Narrowly dispersed poly(methyl methacrylate) (PMMA) was used as the calibration standard. The flow rate of eluent was 0.5 mL/min. The molecule weight distribution curve is shown in Figure S1 in the Supporting Information (SI). The number-average and weight-average molecular weights of the PBCE were 38 and 76 kg/mol, respectively.

2.3.2 Nuclear magnetic resonance (NMR)

The chemical structure of the PBCE was characterized by NMR, using a Bruker Advance 400 instrument. The samples were dissolved in deuterated chloroform with a concentration of 10 g/L. The solution was shaken for 2 hours to ensure dissolution. The ^{1}H NMR spectrum was collected at room temperature. The composition of the polymer is summarized in Table S1.

2.3.3 Differential scanning calorimetry (DSC)

The crystallization and melting behavior of PBCE was studied using a Perkin Elmer DSC 8500. The instrument was calibrated with indium before measurement. The sample was heated to 220 °C and maintained for 3 minutes to eliminate the thermal history. Then the sample was cooled to 0 °C and reheated to 220 °C.

The heating and cooling rate was 10 °C/min. To study the effect of cooling rate, samples were cooled from 220 °C to 0 °C at 10, 20, 30, 40, 50, and 100 °C/min and with ballistic cooling.

2.3.4 Wide angle X-ray scattering (WAXS)

The 2D WAXS pattern of the oriented PBCE sample was measured using a Xeuss 2.0 X-ray diffraction system (Xenocs, France). The instrument was equipped with a microfocus CuKα radiation and a 2D semiconductor detector (Pilatus 300K, Dectris). The stretched PBCE specimen was mounted on a homemade holder to ensure the X-ray was perpendicular to the specimen. To cover a broader scattering angle and a high signal/noise ratio, the sample was exposed for 5 hours with 4 different detector positions with a fixed sample to detector distance (106.85 mm). The samples with different cooling rates were also characterized by WAXS using a shorter exposure time (30 min) and longer sample-to-detector distance (159.70 mm). The structural variation during stretching and heating of PBCE was monitored by WAXS. For the stretching experiment, the sample was stretched at 100 °C on a Linkam TST 350 tensile stage. For the heating, a Linkam HFSX350 was used to control the temperature (±1 ºC). The exposure time was 30 min.

To explore the origin of the double melting peaks, in-situ WAXS experiments were carried out in beamline 1W2A in the Beijing synchrotron radiation facility (BSRF). A MAR CCD detector with a resolution of 2048 pixel × 2048 pixel was used for data collection. The distance between the sample and the detector is 104.90 mm.

To compare the experimental with the calculated WAXS curve of PBCE, the 1D WAXS profile of unoriented PBCE was collected on a Rigaku Smartlab diffractometer operated in reflection mode.

2.3.5 Computer simulations and refinement

The molecular modeling of PBCE was carried out on the Avogadro (version 1.2) platform.[39] The initial model was constructed by high precision conformation energy optimization by CP2K (version 9.1),[40] in which the B97M-V functional and TZVP basis set was used.[41, 42] MultiWFN was also used for special input file generation.[43]

After extracting the intensity of the reflections, a hkl format file was manually generated. The atomic position in the unit cell was refined by Olex2-1.5, by adjusting the torsional angle of the polymer chain.[44] The

2D WAXS pattern and 1D WAXS profile of the refined structure were simulated according to the structure factor using a home-written program.

3. Result and discussion

3.1 Basic characterization of PBCE

The molecular structures of PBCE and two isomers of 1,4-cyclohexylene are illustrated in Figure 1(a). Normally, mixed isomers reduce the regularity of the chains, and cause a depression in melting temperature (T_m) and degree of crystallinity.[13, 45] When PBCE contains nearly 100 % trans- isomers, the T_m can reach ~170 ºC, and the crystallinity is ~40%.[4] The ^{1}H NMR spectrum is showed in Figure 1(b). The chemical shifts of the hydrogen on the butanediol are 1.7 (**b**) and 4.1 ppm (**a**). The peaks at 1.45 (**d**) and 2.05 (**c**) ppm are associated with the H in the cyclohexylene unit. Magnification of the region 2.1 ~ 2.6 ppm indicates the different isomers: trans for 2.27 ppm and cis for 2.46 ppm. Their relative amounts were calculated by integration of the peaks, showing that the PBCE studied contains 97 % trans isomer. Figure 1(c) shows the cooling and second heating DSC curves of the sample. The crystallization temperature is 146.4 ºC. Two endothermic peaks are observed in the heating curve, T_{m1}= 162.6 ºC and T_{m2} = 167.9 ºC. The double-meting behavior may be due to a polymorphic structure or a melting and recrystallization process, which will be discussed later. The thermal behavior is similar to the previous report.[4]

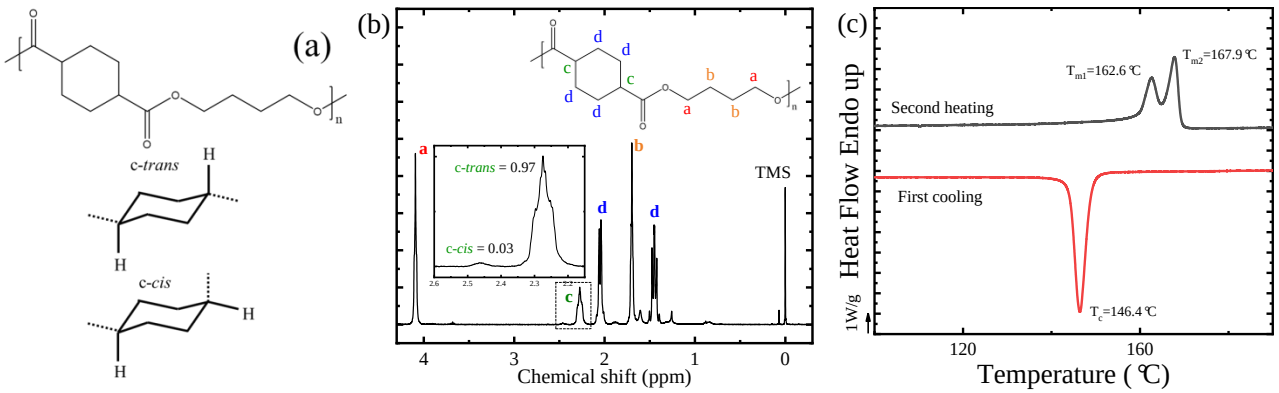

Figure 1. (a) The molecular structure of PBCE and the *cis* and *trans* isomer of 1,4-Cyclohexanedicarboxylic unit. (b) The ^{1}H NMR spectrum of PBCE. (c) DSC cooling and second heating curves of PBCE.

According to the previous work,[8] PBCE shows evidence of polymorphism. To give more detailed information, we studied the WAXS features of samples with different thermal histories: quenched in a cold

mold, slowly cooled (4 ºC/min), and stretch films. Figure 2(a) ~ (c) show the 2D WAXS pattern and Figure 2(d) shows the 1-D intensity profiles. It is clear that the slowly cooled and stretched samples share the same crystal structure, while the quenched sample exhibits a different structure. Since the stretched sample was obtained by stretching the quenched film at 100 ºC, we expect that the crystals in the stretched/slowly cooled samples are more stable than those in the quenched sample. Thus, the former is named ***α form*** and the latter is named ***β form***.

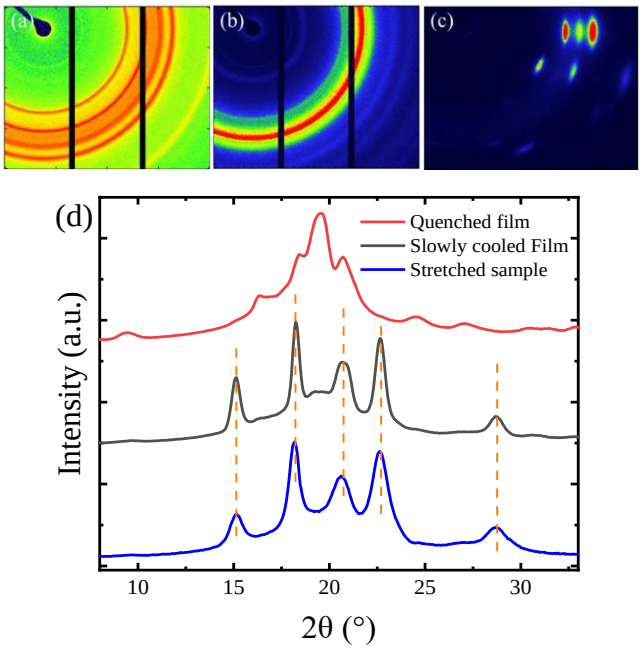

Figure 2. The 2D WAXS patterns of PBCE: (a) Slowly cooled (b) Quenched (c) Stretched sample and intensity profiles (d) 1D WAXS integration curve of (a), (b), (c).

3.2 Fiber pattern and structure analysis

The WAXS pattern of stretched PBCE film (α form) is shown in Figure 3(a). After Fraser correction (Figure 3(b)),[46] the layer lines become "flat", similar to the case of a cylinder detector. The length of the *c*-axis of the unit cell can be estimated by $2\pi/q$ of the first layer line, which is ~13.5 Å. This value most probably corresponds to an all-trans conformation of the butylene unit. A total of 37 diffraction spots located at 6 layer lines were identified. The first task of structure analysis is to index those diffraction spots, which was done by using a home-written code in Python. It turns out that the diffractions of α form can be indexed by a triclinic cell with the following parameters:

a = 5.46 Å, b = 6.89 Å, c = 13.51 Å

α = 138.37°, β = 109.42°, γ = 63.30°

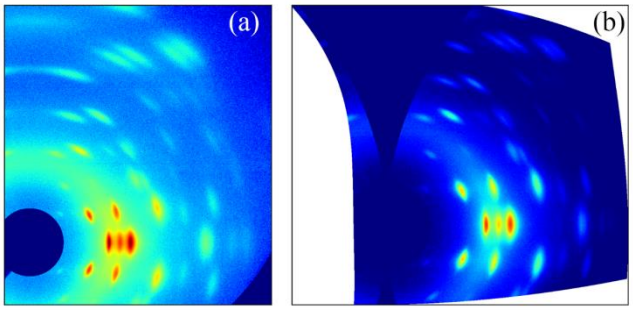

Figure 3. 2D WAXS pattern of PBCE stretched film: (a) raw data (b) after Fraser correction.

The fully indexed fiber pattern is shown in Figure S2 in the SI. The X-ray is strictly perpendicular to the sample, evidenced by the small error in intensity among symmetric diffraction spots (Table S1). Table 1 lists the experimental and calculated values of spacing of (*hkl*) lattice planes, where a good agreement can be found between them. The volume of the unit cell is 301.56 Å^3, and the calculated density of the unit cell is 1.246 g/cm^3 (each unit cell contains one repeating unit). Considering that an inversion center is present in the chain, the most likely space group is P$\bar{1}$.

The conformation of the chain within the unit cell is obtained by computer simulation. We minimized the conformational energy of PBCE α form by CP2K, under the assumption of a periodic boundary condition with the unit cell parameters fixed. The energy-minimized conformation is set as the initial model for refinement. (Figure S3, Table S2 and S3) For the refinement, the observed structure factors of the reflections must be obtained:

$$|F(hkl)|_{obs} = \sqrt{\frac{I(hkl)_{obs}}{KLmpA}}$$

where the observed intensity was corrected for Lorentz factor (L), multiplicity factor (m), polarization factor (p), and absorption factor (A).[14, 15, 47] For the triclinic unit cell, the m is 2 for all *hkl* planes of a triclinic unit cell. However, due to the symmetry of the fiber pattern, the intensity of each reflection is taken from one spot,

and *m* would be corrected by the number of spots. Finally, the *m* for (*hk0*) indices is 1, and 0.5 for (*hkl*, $l \neq 0$). *K* is a scale factor, to normalize the intensity to fit the model.

With those 37 structure factors, the molecular model was refined by Olex2. Since the number of reflections is limited, to reduce the number of free parameters, the atomic displacement parameters of all C and O atoms, represented as U_{eq} in the Olex2, were assumed to be isotropic and set as 0.10. The bond length and bond angle of the molecular chain were also fixed. The torsional angles were adjusted during the refinement to obtain the lowest R-factor, which is defined as:

$$R = \frac{\sum_{hkl} ||F(hkl)|_{obs} - |F(hkl)|_{calc}|}{\sum_{hkl} |F(hkl)|_{obs}}$$

After refinement, the R-factor was reduced to 17.22 %, which is a reasonably low value in polymer structure analysis. The atomic fraction coordinates of PBCE are listed in Table 2. The bond angle and the torsional angle of the chain are listed in Table 3. As expected, each unit cell contains one repeating unit and the butylene unit exhibits an all-trans conformation. The fractional coordinates of the inverse centers within the primitive unit cell are (0, 0, 0), (0.5, 0, 0), (0, 0.5, 0), (0.5, 0.5, 0), (0, 0, 0.5), (0.5, 0, 0.5), (0, 0.5, 0.5), and (0.5, 0.5, 0.5). The line repetition symmetry group of *α*-PBCE belongs to *ti*. The cyclohexane rings have a chair-like conformation. The labels of the atoms in the PBCE structure unit are indicated in Figure 4. The crystal structure of the PBCE *α* form is illustrated in Figure 5.

Table 1. Observed and calculated d-spacings and structure factors of the PBCE *α* form.

h	*k*	*l*	d_{obs} (Å)*	d_{calc} (Å)	$\|F_{obs}\|$*	$\|F_{calc}\|$
1	0	0	4.88	4.88	45.50	39.58
0	1	0	4.33	4.33	27.80	30.69
1	1	0	3.93	3.92	61.74	61.84
2	1	0	} 2.49	2.50	} 24.90	15.76
2	0	0		2.44		11.07
1	2	0	2.26	2.27	6.40	8.05
0	2	0	2.16	2.17	6.52	12.86
0	0	1	8.99	8.97	1.41	1.42
0	-1	1	5.85	5.86	33.23	27.51
1	0	1	} 4.28	4.30	} 41.20	25.02
-1	0	1		4.28		27.94
0	1	1	3.12	3.13	42.54	45.31
-1	-2	1	2.72	2.73	7.64	10.57
-1	1	1	2.38	2.39	16.99	18.44

0	-1	2	5.78	5.78	5.13	5.15
0	0	2	4.50	4.49	4.15	8.07
1	0	2	} 3.31	3.31	} 13.23	12.72
-1	0	2		3.29		10.48
-1	-2	2	3.17	3.19	6.84	9.00
-2	-1	2	2.69	2.69	4.76	3.58
1	-2	2	2.15	2.14	9.88	9.20
0	-1	3	4.26	4.25	6.65	4.30
-1	-1	3	3.81	3.84	17.79	17.21
-1	-2	3	3.36	3.37	4.83	9.08
0	-2	3	3.07	3.08	11.65	9.42
1	0	3	} 2.53	2.56	} 7.45	2.33
-2	-2	3		2.55		4.72
-1	0	3		2.54		5.80
1	-2	3	2.20	2.19	7.55	7.47
-1	-2	4	} 3.11	3.13	} 9.29	8.27
0	-1	4		3.07		5.00
-1	-1	4	} 2.90	2.90	} 15.03	2.51
0	-2	4		2.89		13.99
-2	-2	4	2.41	2.44	9.05	6.45
0	0	4	2.24	2.24	3.62	4.52
-2	-1	4	2.14	2.16	6.05	7.20
0	-2	5	2.52	2.51	11.90	11.30
0	-1	5	2.35	2.35	2.11	2.60
-1	-1	5	} 2.25	2.27	} 13.23	14.18
-1	-3	5		2.27		8.49
-2	-2	5	2.18	2.19	16.17	13.57
0	-3	5	2.04	2.03	13.95	17.74
1	-1	5	} 1.99	1.99	} 14.53	13.96
1	-2	5		1.96		22.78

*Some diffraction peaks overlap and cannot be distinguished. The *d*-spacing and structure factor of the overlapped peaks are summed up.

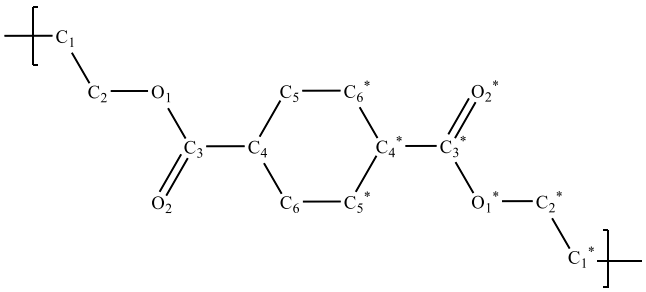

Figure 4. The labels of the atoms in Table 2. (* represent the symmetrically equivalent atom)

Table 2. Atomic Fraction Coordinates of *α*-PBCE Crystals.

Serial	Atom number	x	y	z
1	C1	-0.06185	0.00387	0.04453
2	H1a	-0.19055	0.20797	0.11702
3	H1b	-0.16267	-0.14236	-0.02233

4	C2	0.15161	-0.07312	0.12428
5	H2a	0.3032	-0.25387	0.05746
6	H2b	0.22178	0.09781	0.20867
7	C3	0.19081	-0.1953	0.25309
8	C4	0.04237	-0.12688	0.35623
9	H4	-0.11177	-0.20837	0.30178
10	C5	-0.07356	0.22252	0.49256
11	H5a	0.07517	0.30944	0.54742
12	H5b	-0.19606	0.32048	0.45987
13	C6	0.22902	-0.28608	0.40598
14	H6a	0.38502	-0.21134	0.45887
15	H6b	0.29717	-0.50677	0.31921
16	O1	0.02363	-0.13297	0.17509
17	O2	0.43463	-0.29601	0.23029

The unit cell parameters: a = 5.46 Å, b = 6.89 Å, c = 13.51 Å, α = 138.37°, β = 109.42°, γ = 63.30°. The space group is $P\bar{1}$. The unit cell contains 34 atoms (17 atoms are listed due to the symmetry). The label of H indicates the bonded C atoms.

Table 3. The bond angle and the torsion angle of the PBCE chain in the unit cell.

Bond/Torsion angle atoms	Bond/Torsion Angle
C1* - C1 - C2	112.55°
C1 - C2 - O1	108.09°
C2 - O1 - C3	114.31°
O1 - C3 - O2	116.23°
C4 - C3 - O1	113.74°
C4 - C3 - O2	130.04°
C6 - C4 - C3	111.05°
C5 - C4 - C3	111.33°
C6 - C4 - C5	110.26°
C4 - C6 - C5*	110.64°
C4 - C5 - C6*	110.27°
C4 - C5 - C6 - C4*	57.75°
C5* - C6 - C4 - C3	-178.38°
C5* - C6 - C4 - C5	57.74°
C6* - C5 - C4 - C3	178.76°
C6* - C5 - C4 - C6	-57.53°
C6 - C4 - C3 - O2	-16.80°
C5 - C4 - C3 - O2	106.47°
C6 - C4 - C3 - O1	163.36°
C5 - C4 - C3 - O1	-73.37°
O2 - C3 - O1 - C2	-24.07°
C4 - C3 - O1 - C2	155.79°
C3 - O1 - C2 - C1	177.92°
O1 - C2 - C1 - C1*	-166.43°
C2 - C1 - C1* - C2*	180.00°

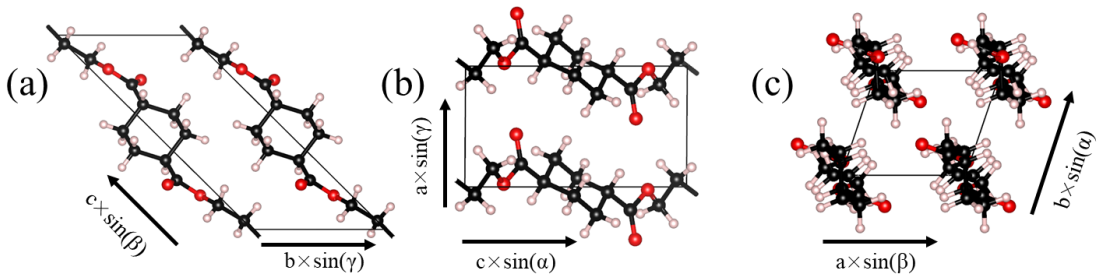

Figure 5. The crystal structure of *α*-PBCE. (a) projection along the a-axis. (b) projection along the b-axis. (c) projection along the c-axis.

To verify the accuracy of the proposed crystal structure, we compared the experimental 2D WAXS pattern with the calculated 2D WAXS pattern based on the unit cell model (Figure 6). The calculated structure factors of the lattice planes of our model are exported from VESTA (Ver. 3.5.8).[48] Judged by the naked eye, the two patterns are almost the same. In fact, in Figure 6b, 91 reflections were plotted, much more than the number of distinguishable peaks in Figure 6(a) (37). However, the rest of them are very weak and are not visible in the scale of the graph. We also plotted the calculated 1D WAXS curve with the experimental curve. A good agreement between them is also achieved.

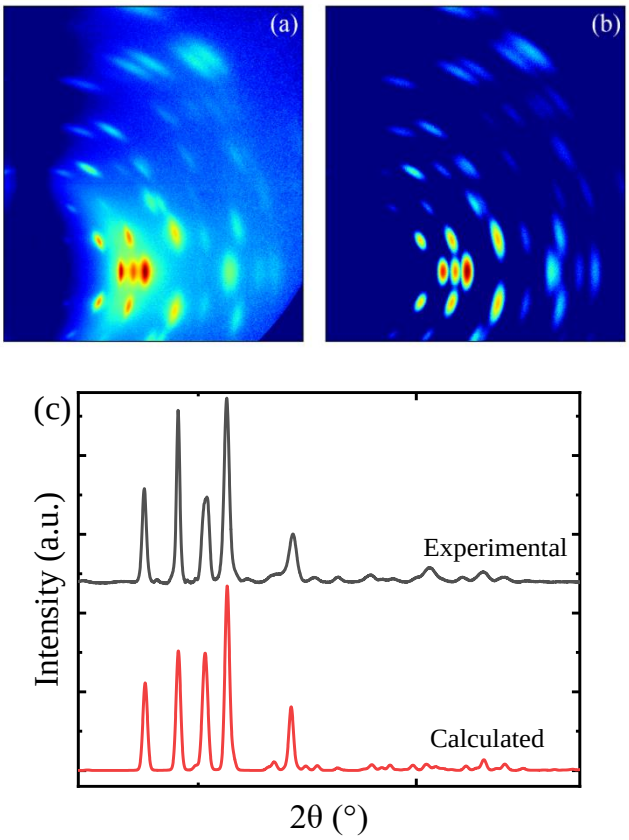

Figure 6. Experimental (a) and calculated (b) 2D WAXS pattern of PBCE *α* form. The experimental pattern is modified from Figure 3(a) after correction for the Lorentz factor, polarization factor, and absorption factor. The simulated spots are convoluted by 2D Gaussian function assuming standard deviation (σ) of 0.4º in 2θ and 3.2º in azimuth angle. (c) Comparison of the observed and simulated 1D WAXS profiles using a Gaussian convolution with σ = 0.2º. Scattering from the amorphous phase was subtracted from the experimental profile.

3.3 Polymorphism and polymorphic transition in PBCE

As shown in Figure 2, the crystalline structure of PBCE is strongly influenced by the cooling condition. To further study the impact of cooling rate, WAXS profiles of PBCE samples crystallized under different cooling rates are shown in Figure 7a. The cooling DSC curves are presented in Figure 7(b). The sample crystallized at a lower temperature when the cooling rate was higher. The intensities of the diffraction peaks of the *β* form gradually increase with rising cooling rates. This indicates that the *β* form develops at larger undercoolings and is thus probably a metastable phase.

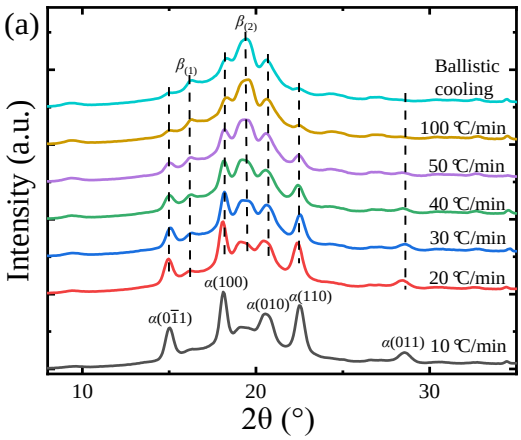

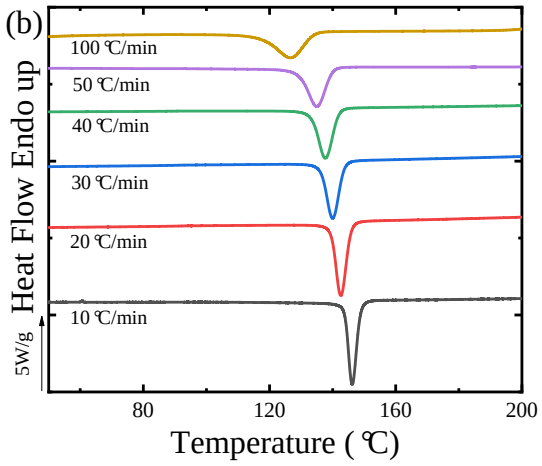

Figure 7. (a) 1D WAXS curve of PBCE under different cooling rates. (b) DSC cooing curve with different cooling rates.

A metastable phase can transform into a stable phase under given conditions. The DSC melting curves of α and β form are presented in Figure S4. Both of them show double melting peaks, which could be attributed to a crystal transition or a melting-recrystallization process.[49] To study the origin of the double melting behavior, a DSC protocol was designed: the samples with the same initial structures were heated at different heating rates (5, 10, 20, 30, 50, 70, 100, and 150 °C/min). As shown in Figures S5 and S6, for both the two samples, with increasing heating rates, the area of the low-temperature peak increased, and the area of the high-temperature peak decreased. When the heating rate exceeds a certain value, only one peak can be observed. This indicates the double melting peaks in PBCE is a melting-recrystallization process.[50, 51]

To further explore whether temperature can trigger the transition, the WAXS patterns of α and β form crystals at different temperatures are measured. As shown in Figure 8a, for the α phase, the WAXS profiles show clear and continuous changes with temperature. Especially, the (010), (110), and (011) reflections shift to lower q with temperature, indicating a non-trivial lattice expansion. However, the intensity of diffraction rings remains relatively unchanged. This implies that the unit cell of the α phase crystallites undergoes thermal expansion without substantial alteration in chain conformation. On the other hand, as shown in Figure 8(b), both the position and intensity of the reflections of the β phase changes with temperature. Further analysis of the variation of β phase is not possible because of the lack of crystallographic information. When the samples were cooled to 25 ºC from 160 ºC, the WAXS recovered completely to the original curve, indicating that both

α and β phases are stable till 160 ºC, which is very close to the T_m. We further carried out in-situ WAXS experiments using synchrotron radiation. The temperature variation program is shown in Scheme S1 and the results are presented in Figure S7 in the SI. The results indicate that during heating the β phase directly transforms to the melt state. No temperature-triggered β to α was observed for the investigated heating rate (10 ºC/min).

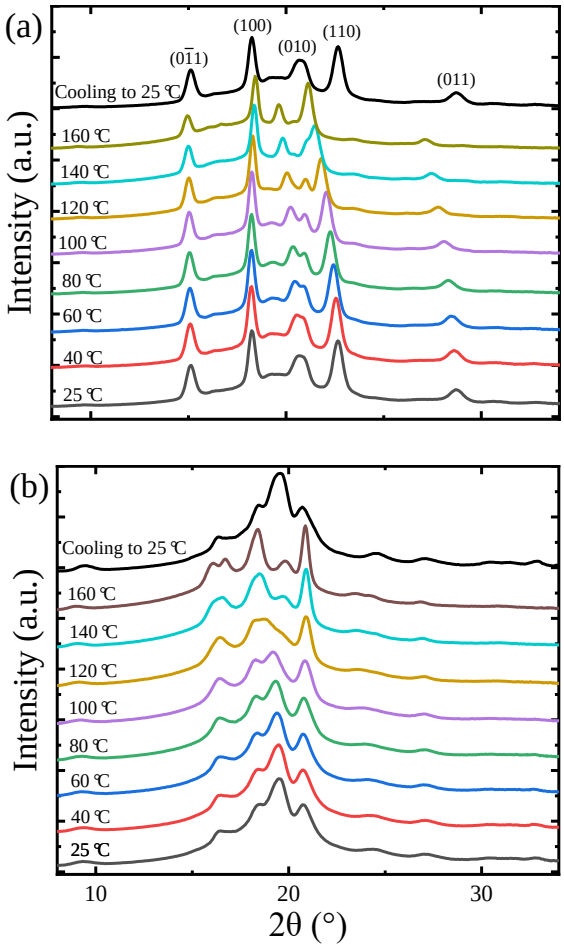

Figure 8. WAXS profiles of PBCE α phase (a) and β phase (b) at different temperatures. The samples were heated to different temperatures and cooled to 25 ºC after reaching 160 ºC.

To quantitatively explore the lattice deformation, temperature-dependent fiber diffraction patterns were used to collect more reflections. In the fiber patterns (Figure 9a), the changes in the equatorial diffraction peaks are very obvious. The d-spacings of various reflections are plotted in Figure 9(b-e). The changes for different planes are not the same: d(010), d(110), d(001), d(011), d(0$\bar{1}$1) and d(102) increase with temperature,

while d(100), d(0$\bar{1}$2), d(0$\bar{1}$3), d($\bar{1}\bar{1}$3), and d(0$\bar{2}$3) have the opposite trend. With increasing temperature, the overlapped (-101) and (101) diffractions split.

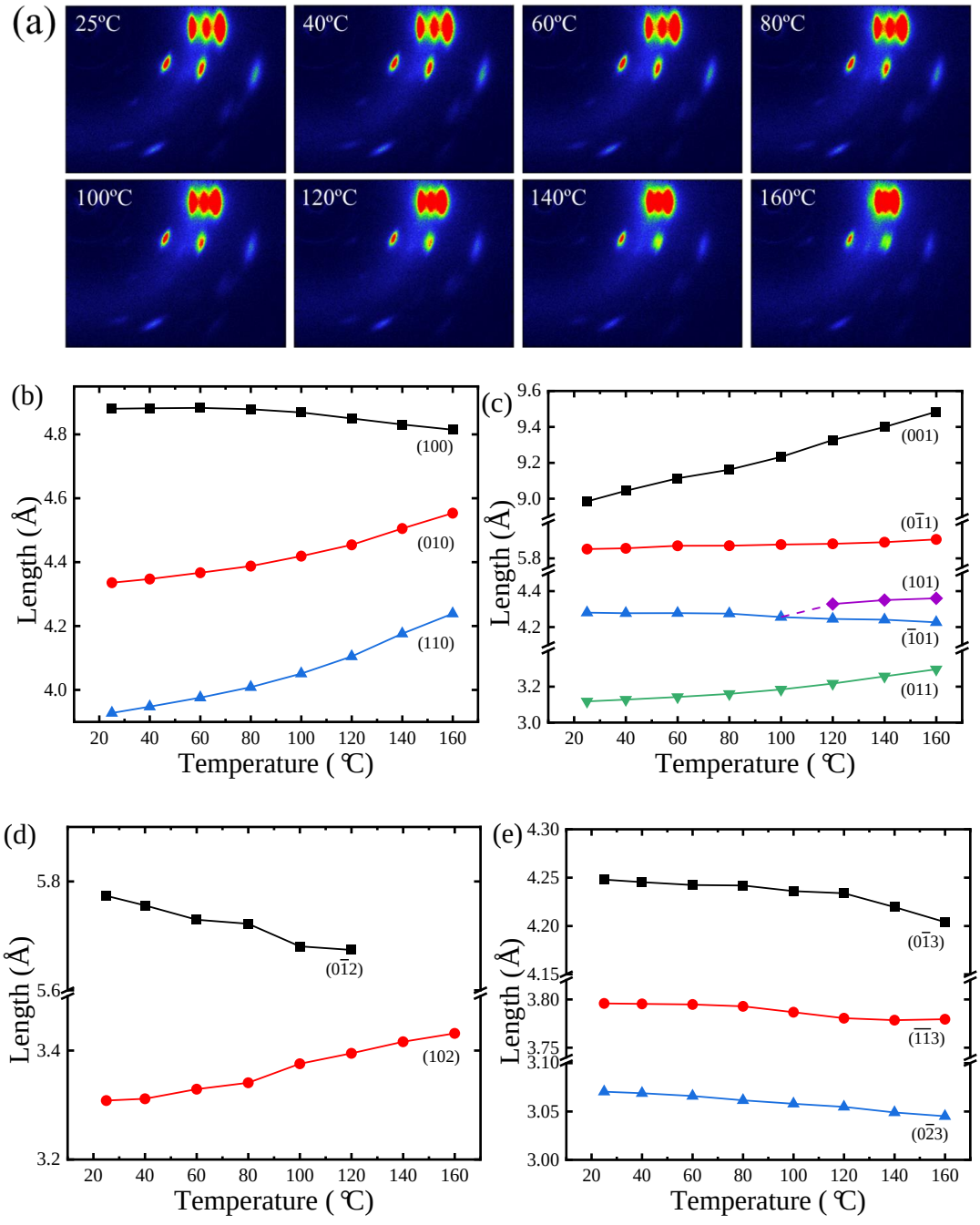

Figure 9. The WAXS patterns of PBCE fiber at different temperatures (a) and the d-spacings of planes on the equator (b) and on different layer lines (c-e) as a function of temperature.

The unit cell parameters of the PBCE α form were calculated according to the d-spacings shown in Figure 9. Each set of parameters was optimized through error minimization between the observed and

calculated d-spacings. The temperature-dependent unit cell parameters are presented in Figure 10. It is observed that *a* and *b*, associated with the interchain packing, increase with temperature while *c*, associated with the repeating length and conformation, shows a decrease. The decreasing *c* reflects a change in the torsion angle of the trans-conformation. The chain conformation may deviate more from the ideal all-trans conformation, resulting in a slight decrease in the axial length of the molecular chain as the temperature increases. With temperature increase, the α and γ decrease slightly, while β remains essentially unchanged. The overall effect is that the volume of the unit cell increases from 300 to 316 Å^3. The thermal expansion coefficient of the unit cell can be calculated by:[52]

$$\alpha_V = \frac{1}{V}\left(\frac{\partial V}{\partial T}\right)_p$$

$$\alpha_x = \frac{1}{x}\left(\frac{\partial x}{\partial T}\right)_p$$

where V is the cell volume and x is a unit cell parameter (length or angle). The variation of unit cell parameters is almost linear, so the partial derivative relative to temperature can be considered as the slope of the fitting function. The thermal expansion coefficients of six parameters and unit cell volume are listed below:

$$\alpha_a = 1.12 \times 10^{-4}K^{-1}, \alpha_b = 1.50 \times 10^{-4}K^{-1}, \alpha_c = -5.26 \times 10^{-5}K^{-1}$$

$$\alpha_\alpha = -1.64 \times 10^{-4}K^{-1}, \alpha_\beta = 9.60 \times 10^{-6}K^{-1}, \alpha_\gamma = -3.66 \times 10^{-4}K^{-1}$$

$$\alpha_V = 4.22 \times 10^{-4}K^{-1}$$

According to the literature, the α_V of the unit cell is 3.45×10^{-4} K^{-1} for isotactic polypropylene (iPP, α phase)[52], 0.5 ~ 2.5×10^{-4} K^{-1} for polyethylene (PE, 50 to 250 K),[53] 1.4×10^{-4} K^{-1} for PHB,[54] and 2.13×10^{-4} K^{-1} for PBT.[55] Compared with those polymers, α_V of α-PBCE is relatively higher: twice the values of PBT. This manifests a clear difference between the benzene ring and cyclohexane rings in the backbone, with the latter having stronger molecular vibrations.

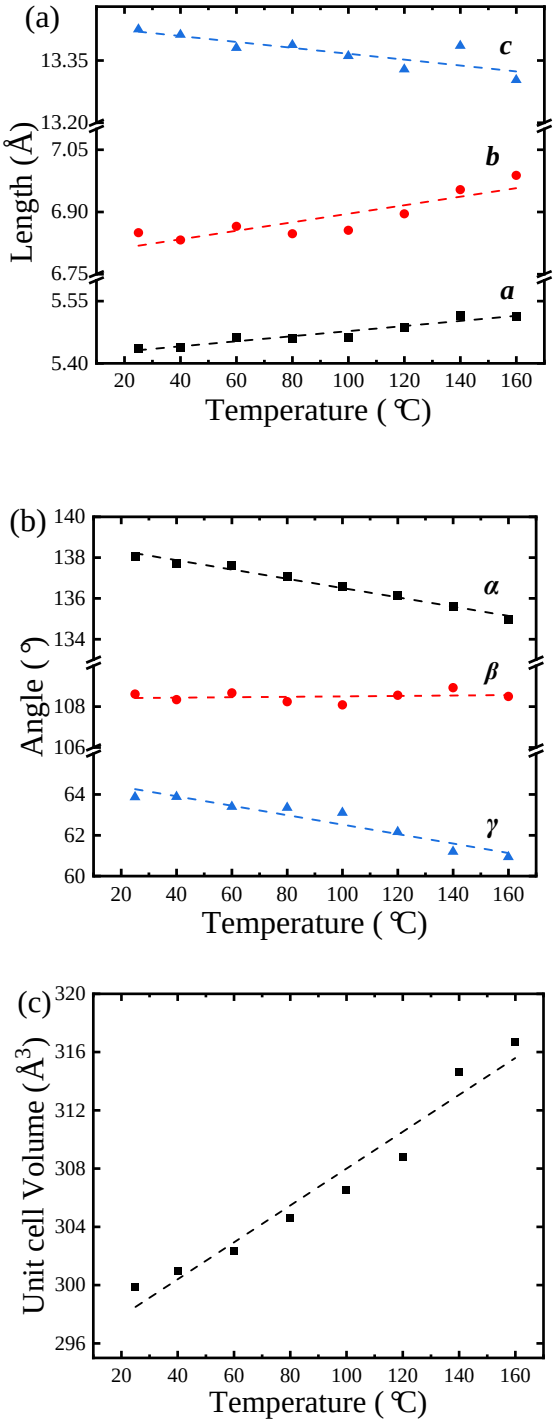

Figure 10. The unit cell parameters of PBCE *α* form during heating: (a) *a*, *b*, *c*; (b) *α*, *β*, *γ*; (c) the volume of the unit cell. The cell parameters and volume at different temperature are fitted by linear function.

Since the oriented sample was obtained by stretching hot-pressed film (*β* form), it is likely that the *β* form transforms into the *α* form during deformation. To understand this process, WAXS patterns with different strains in the stretching process at 100 ºC are shown in Figure 11. With increasing strain, the Debye rings

became arcs, indicating that the crystalline structure becomes oriented. 1D WAXS profiles show that the sample is mainly composed of α form when the strain exceeds 200 %.

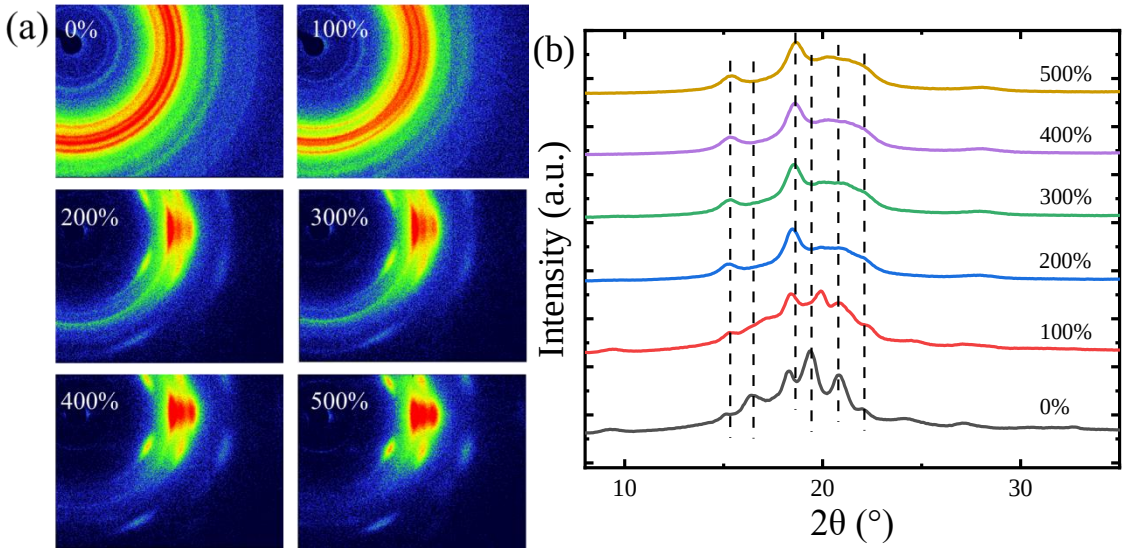

Figure 11. In situ WAXS patterns (a) and intensity profiles (b) of the PBCE with different stains during stretching at 100 ºC. The azimuthal integration region is -35º to 35º.

An interesting WAXS pattern is observed for a strain of 100%. The pattern is magnified in Figure 12(a). The scattering features in the equator and meridian are different. The intensity profiles integrated with different azimuth angles are presented in Figure 12b, which demonstrates the distribution of crystals with different orientations. The WAXS profile along the meridian is almost the same as the unstretched sample. However, the intensity profiles along the equator show the characteristic peaks, (100), (010), and (110) for the α crystal.

The (*hk0*) diffraction on the equator is contributed by crystallites with the chain parallel to the stretching direction. These crystallites already have the "right orientation" and, therefore are likely to undergo plastic deformation, i.e., strain-induced melting and recrystallization.[56-58] On the other hand, the (*hk0*) reflections on the meridian correspond to the crystallites with the chain axis nearly perpendicular to the stretching direction. Thus, the first stage of crystal deformation is rotation/tilt to accommodate the strain. The reflections on the meridian shift to lower angles, suggesting that instead of crystal transition, the crystals undergo lattice expansion. A cartoon is drawn to show the spatially heterogeneous transition.

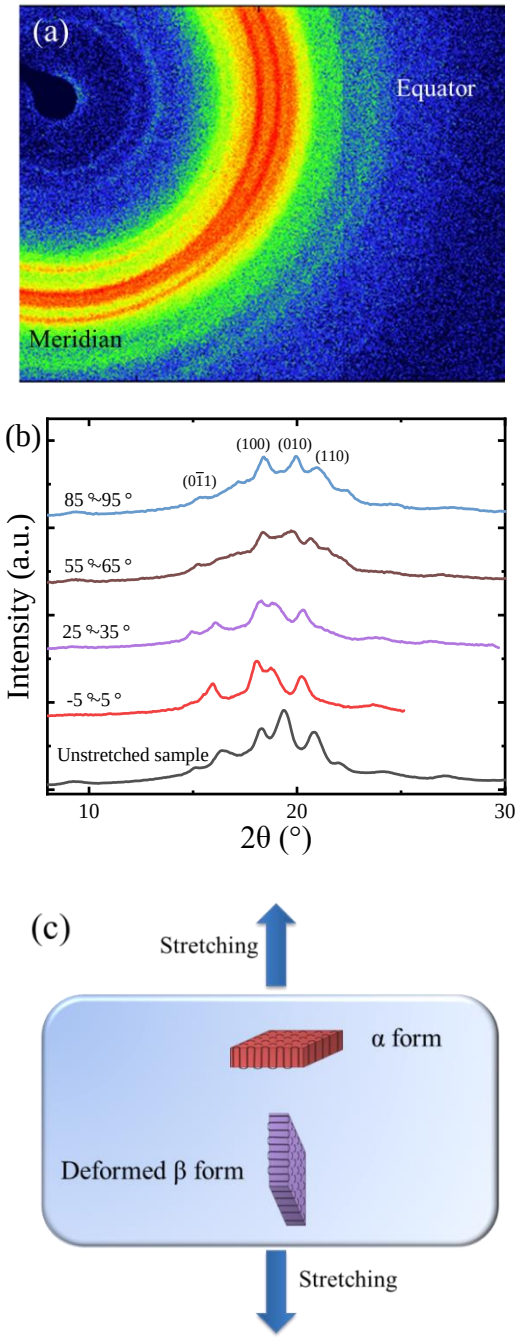

Figure 12. (a) WAXS pattern of PBCE with 100 % strain; (b) intensity profiles integrated with different azimuth ranges (the azimuth on the equator is defined as 0º); (c) a scheme illustrating the early stage of crystal transition of PBCE. The purple crystals contribute to the diffraction in the meridian and the red one to the equator.

The transition between the *α* and *β* forms of PBCE is summarized in Scheme 1. When the PBCE melt is slowly cooled, it predominantly crystalizes into the *α* phase. The *β* phase, on the other hand, is formed under higher cooling rates (kinetically favored at higher undercooling). The *β* phase transforms irreversibly into the

α phase by stretching, indicating the β phase is metastable. However, during heating at 10 ºC/min, the β phase directly melts, without transforming into the α phase. This indicates a monotropic polymorphism of the two structures.

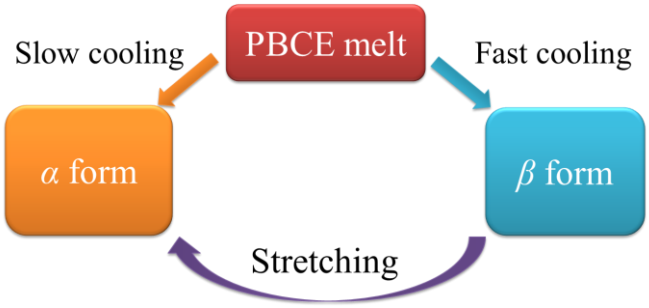

Scheme 1. The crystal form transition in PBCE.

4. Conclusion

The crystalline structure and polymorphic transition of PBCE were systematically studied. Two crystalline phases were identified, namely, the α and β forms. The α form can be obtained by slow cooling or by stretching the β form. By the fiber pattern analysis, the crystal structure of the α form was solved. It has a triclinic unit cell with a $P\bar{1}$ space group: a = 5.46 Å, b = 6.89 Å, c = 13.51 Å, α = 138.37°, β = 109.42°, γ = 63.30°. The line repetition symmetry group of α-PBCE belongs to *ti*. With fast cooling from the melt, PBCE crystallized into another form (β form). The crystal structure of β form was not solved because of the difficulty in obtaining oriented samples due to the stretching-induced β-α transition. WAXS results indicated a significant lattice distortion with temperature for both α and β forms. The volumetric thermal expansion coefficient of PBCE α form was twice that of PBT, which may be related to the nonplanar vibrations of the cyclohexane ring in the backbone. The β to α stretch-induced transition exhibited a spatially heterogeneous feature, with the scattering signal on the equator transformed "earlier" than that on the meridian, manifesting the impact of hierarchical structure on the micromechanical response.

Supporting Information

GPC results of the PBCE sample, the indexed 2D WXRD of stretched PBCE sample, the intensities of symmetrically equivalent diffraction spots, the atomic fractional coordinate, bond angle, and torsion angle,

unit cell model of the energy-minimized model (before refinement), the DSC results of first heating and second heating of hot-pressed film, DSC protocol and heating curves of PBCE with different crystal forms, the thermal protocol and in-situ WAXS results of the α and β PBCE.

Notes

The authors declare no competing financial interest.

Acknowledgments

This work is supported by the National Natural Science Foundation of China (22273113). We thank Dr. Xiang Hao of ICCAS for the resistance in data analysis and Prof. Zhihong Li of IHEP for the assistance in in-situ WAXS measurements. The BSRF is acknowledged for providing the beamtime.

References

(1) Zhang, Q. N.; Song, M. Z.; Xu, Y. N.; Wang, W. C.; Wang, Z.; Zhang, L. Q. Bio-based polyesters: Recent progress and future prospects. *Progress in Polymer Science* **2021**, *120*. DOI: 10.1016/j.progpolymsci.2021.101430.

(2) Zia, K. M.; Noreen, A.; Zuber, M.; Tabasum, S.; Mujahid, M. Recent developments and future prospects on bio-based polyesters derived from renewable resources: A review. *International Journal of Biological Macromolecules* **2016**, *82*, 1028-1040. DOI: 10.1016/j.ijbiomac.2015.10.040.

(3) Berti, C.; Celli, A.; Marchese, P.; Marianucci, E.; Barbiroli, G.; Di Credico, F. Influence of molecular structure and stereochemistry of the 1,4-cyclohexylene ring on thermal and mechanical behavior of poly(butylene 1,4-cyclohexanedicarboxylate). *Macromolecular Chemistry and Physics* **2008**, *209* (13), 1333-1344. DOI: 10.1002/macp.200800125.

(4) Gigli, M.; Lotti, N.; Gazzano, M.; Siracusa, V.; Finelli, L.; Munari, A.; Dalla Rosa, M. Fully Aliphatic Copolyesters Based on Poly(butylene 1,4-cyclohexanedicarboxylate) with Promising Mechanical and Barrier Properties for Food Packaging Applications. *Industrial & Engineering Chemistry Research* **2013**, *52* (36), 12876-12886. DOI: 10.1021/ie401781d.

(5) Zhang, X.; Liu, Q.; Shi, J.; Ye, H.; Zhou, Q. Distinctive Tensile Properties of the Blends of Poly (l-lactic acid)(PLLA) and Poly (butylene succinate)(PBS). *Journal of Polymers and the Environment* **2018**, *26*, 1737-1744.

(6) Guidotti, G.; Soccio, M.; Siracusa, V.; Gazzano, M.; Munari, A.; Lotti, N. Novel Random Copolymers of Poly(butylene 1,4-cyclohexane dicarboxylate) with Outstanding Barrier Properties for Green and Sustainable Packaging: Content and Length of Aliphatic Side Chains as Efficient Tools to Tailor the Material's Final Performance. *Polymers* **2018**, *10* (8), Article. DOI: 10.3390/polym10080866.

(7) Genovese, L.; Dominici, F.; Gigli, M.; Armentano, I.; Lotti, N.; Fortunati, E.; Siracusa, V.; Torre, L.; Munari, A. Processing, thermo-mechanical characterization and gas permeability of thermoplastic starch/poly(butylene trans-1,4-cyclohexanedicarboxylate) blends. *Polymer Degradation and Stability* **2018**, *157*, 100-107. DOI: 10.1016/j.polymdegradstab.2018.10.004.

(8) Guidotti, G.; Burzotta, G.; Soccio, M.; Gazzano, M.; Siracusa, V.; Munari, A.; Lotti, N. Chemical Modification of Poly(butylene trans-1,4-cyclohexanedicarboxylate) by Camphor: A New Example of Bio-Based Polyesters for Sustainable Food Packaging. *Polymers* **2021**, *13* (16). DOI: 10.3390/polym13162707.

(9) Guidotti, G.; Soccio, M.; Argentati, C.; Luzi, F.; Aluigi, A.; Torre, L.; Armentano, I.; Emiliani, C.; Morena, F.; Martino, S.; et al. Novel Nanostructured Scaffolds of Poly(butylene trans-1,4-cyclohexanedicarboxylate)-Based Copolymers with Tailored Hydrophilicity and Stiffness: Implication for Tissue Engineering Modeling. *Nanomaterials* **2023**, *13* (16). DOI: 10.3390/nano13162330.

(10) Liu, F.; Qiu, J.; Wang, J. G.; Zhang, J. W.; Na, H. N.; Zhu, J. Role of cis-1,4-cyclohexanedicarboxylic acid in the regulation of the structure and properties of a poly(butylene adipate-co-butylene 1,4-cyclohexanedicarboxylate) copolymer. *Rsc Advances* **2016**, *6* (70), 65889-65897. DOI: 10.1039/c6ra13495e.

(11) Liu, F.; Zhang, J. W.; Wang, J. G.; Liu, X. Q.; Zhang, R. Y.; Hu, G. H.; Na, H. N.; Zhu, J. Soft segment free thermoplastic polyester elastomers with high performance. *Journal of Materials Chemistry A* **2015**, *3* (26), 13637-13641. DOI: 10.1039/c5ta03325j.

(12) Liu, W.; Zhang, R. Y.; Huang, M. M.; Dong, X.; Xu, W.; Wang, Y. B.; Hu, G. H.; Zhu, J. Synthesis and shape memory property of segmented poly(ester urethane) with poly(butylene 1,4-cyclohexanedicarboxylate) as the soft segment. *Rsc Advances* **2016**, *6* (98), 95527-95534. DOI: 10.1039/c6ra16325d.

(13) Liu, F.; Chi, D. Q.; Na, H. N.; Zhu, J. Isothermal Crystallization Kinetics and Crystalline Morphologies of Poly(butylene adipate-co-butylene 1,4-cyclohexanedicarboxylate) Copolymers. *Chinese Journal of Polymer Science* **2018**, *36* (6), 756-764. DOI: 10.1007/s10118-018-2051-9.

(14) De Rosa, C.; Auriemma, F. *Crystals and crystallinity in polymers: diffraction analysis of ordered and disordered crystals*; John Wiley & Sons, 2013.
(15) Tashiro, K. *Structural Science of Crystalline Polymers*; Springer, 2022.
(16) De Rosa, C.; Auriemma, F.; Vinti, V. On the form II of syndiotactic polypropylene. *Macromolecules* **1998**, *31* (21), 7430-7435. DOI: 10.1021/ma980789m.
(17) DeRosa, C. Crystal structure of the trigonal modification (alpha form) of syndiotactic polystyrene. *Macromolecules* **1996**, *29* (26), 8460-8465. DOI: 10.1021/ma960905q.
(18) Derosa, C.; Corradini, P. CRYSTAL-STRUCTURE OF SYNDIOTACTIC POLYPROPYLENE. *Macromolecules* **1993**, *26* (21), 5711-5718. DOI: 10.1021/ma00073a028.
(19) Ho, R. M.; Cheng, S. Z. D.; Hsiao, B. S.; Gardner, K. H. CRYSTAL MORPHOLOGY AND PHASE IDENTIFICATION IN POLY(ARYL ETHER KETONE)S AND THEIR COPOLYMERS .3. POLYMORPHISM IN A POLYMER CONTAINING ALTERNATED TEREPHTHALIC ACID AND ISOPHTHALIC ACID ISOMERS. *Macromolecules* **1995**, *28* (6), 1938-1945. DOI: 10.1021/ma00110a030.
(20) Lotz, B.; Miyoshi, T.; Cheng, S. Z. D. 50th Anniversary Perspective: Polymer Crystals and Crystallization: Personal Journeys in a Challenging Research Field. *Macromolecules* **2017**, *50* (16), 5995-+. DOI: 10.1021/acs.macromol.7b00907.
(21) Nakama, Y.; Hayano, S.; Tashiro, K. Influence of Tacticity on the Crystal Structures of Hydrogenated Ring-Opened Poly(norbornene)s. *Macromolecules* **2021**, *54* (17), 8122-8134, Article. DOI: 10.1021/acs.macromol.1c01036.
(22) Tashiro, K.; Guillory, G. A.; Marxsen, S. F.; Kennemur, J. G.; Alamo, R. G. Crystal Structures of Isotactic and Atactic Poly(1-pentamethylene alcohol). *Macromolecules* **2023**, *56* (15), 5993-6002, Article. DOI: 10.1021/acs.macromol.3c01060.
(23) Tashiro, K.; Ono, K.; Minagawa, Y.; Kobayashi, M.; Kawai, T.; Yoshino, K. STRUCTURE AND THERMOCHROMIC SOLID-STATE PHASE-TRANSITION OF POLY(3-ALKYLTHIOPHENE). *Journal of Polymer Science Part B-Polymer Physics* **1991**, *29* (10), 1223-1233. DOI: 10.1002/polb.1991.090291007.
(24) Chatani, Y.; Okita, Y.; Tadokoro, H.; Yamashita, Y. STRUCTURAL STUDIES OF POLYESTERS .3. CRYSTAL STRUCTURE OF POLY-EPSILON-CAPROLACTONE. *Polymer Journal* **1970**, *1* (5), 555-+. DOI: 10.1295/polymj.1.555.
(25) Chatani, Y.; Suehiro, K.; Okita, Y.; Tadokoro, H.; Chujo, K. STRUCTURAL STUDIES OF POLYESTERS .I. CRYSTAL STRUCTURE OF POLYGLYCOLIDE. *Makromolekulare Chemie-Macromolecular Chemistry and Physics* **1968**, *113* (APR), 215-&.
(26) Daubeny, R. D.; Bunn, C. W. THE CRYSTAL STRUCTURE OF POLYETHYLENE TEREPHTHALATE. *Proceedings of the Royal Society of London Series a-Mathematical and Physical Sciences* **1954**, *226* (1167), 531-542.
(27) Ihn, K. J.; Yoo, E. S.; Im, S. S. STRUCTURE AND MORPHOLOGY OF POLY(TETRAMETHYLENE SUCCINATE) CRYSTALS. *Macromolecules* **1995**, *28* (7), 2460-2464. DOI: 10.1021/ma00111a045.
(28) Niu, D. Y.; Wang, H.; Liu, B.; Xu, P. W.; Tashiro, K.; Yang, C. M.; Ma, P. M. Crystal Structure of Poly(glycolic acid) β Form. *Macromolecules* **2023**, *56* (21), 8767-8775. DOI: 10.1021/acs.macromol.3c01909.
(29) Sato, H.; Ando, Y.; Dybal, J.; Iwata, T.; Noda, I.; Ozaki, Y. Crystal structures, thermal behaviors, and C-H•••O=C hydrogen bondings of poly(3-hydroxyvalerate) and poly(3-hydroxybutyrate) studied by infrared spectroscopy and X-ray diffraction. *Macromolecules* **2008**, *41* (12), 4305-4312. DOI: 10.1021/ma702222a.
(30) Suehiro, K.; Chatani, Y.; Tadokoro, H. STRUCTURAL STUDIES OF POLYESTERS .6. DISORDERED CRYSTAL-STRUCTURE (FORM-2 OF POLY(BETA-PROPIOLACTONE). *Polymer Journal* **1975**, *7* (3), 352-358. DOI: 10.1295/polymj.7.352.

(31) Tashiro, K.; Kouno, N.; Wang, H.; Tsuji, H. Crystal Structure of Poly(lactic acid) Stereocomplex: Random Packing Model of PDLA and PLLA Chains As Studied by X-ray Diffraction Analysis. *Macromolecules* **2017**, *50* (20), 8048-8065, Article. DOI: 10.1021/acs.macromol.7b01468.
(32) Ueda, A. S.; Chatani, Y.; Tadokoro, H. STRUCTURAL STUDIES OF POLYESTERS .4. MOLECULAR AND CRYSTAL STRUCTURES OF POLY(ETHYLENE SUCCINATE) AND POLY(ETHYLENE OXALATE). *Polymer Journal* **1971**, *2* (3), 387-&. DOI: 10.1295/polymj.2.387.
(33) Wang, H.; Tashiro, K. Reinvestigation of Crystal Structure and Intermolecular Interactions of Biodegradable Poly(3-Hydroxybutyrate) α-Form and the Prediction of Its Mechanical Property. *Macromolecules* **2016**, *49* (2), 581-594. DOI: 10.1021/acs.macromol.5b02310.
(34) Minke, R.; Blackwell, J. POLYMORPHIC STRUCTURES OF POLY(TETRAMETHYLENE ADIPATE). *Journal of Macromolecular Science-Physics* **1979**, *B16* (3), 407-417. DOI: 10.1080/00222347908212305.
(35) Liu, J.; Geil, P. H. Electron diffraction and computer modeling studies of the crystal structure of poly(butylene terephthalate) alpha-form single crystals. *Journal of Macromolecular Science-Physics* **1997**, *B36* (2), 263-280. DOI: 10.1080/00222349708220430.
(36) Koyano, H.; Yamamoto, Y.; Saito, Y.; Yamanobe, T.; Komoto, T. Crystal structure of poly(butylene-2,6-naphthalate). *Polymer* **1998**, *39* (18), 4385-4391. DOI: 10.1016/s0032-3861(97)00618-6.
(37) Mencik, Z. CRYSTAL-STRUCTURE OF POLY(TETRAMETHYLENE TEREPHTHALATE). *Journal of Polymer Science Part B-Polymer Physics* **1975**, *13* (11), 2173-2181. DOI: 10.1002/pol.1975.180131109.
(38) Tashiro, K.; Yamamoto, H.; Yoshioka, T.; Ninh, T. H.; Tasaki, M.; Shimada, S.; Nakatani, T.; Iwamoto, H.; Ohta, N.; Masunaga, H. Hierarchical Structural Change in the Stress-Induced Phase Transition of Poly(tetramethylene terephthalate) As Studied by the Simultaneous Measurement of FTIR Spectra and 2D Synchrotron Undulator WAXD/SAXS Data. *Macromolecules* **2014**, *47* (6), 2052-2061. DOI: 10.1021/ma402041r.
(39) Hanwell, M. D.; Curtis, D. E.; Lonie, D. C.; Vandermeersch, T.; Zurek, E.; Hutchison, G. R. Avogadro: an advanced semantic chemical editor, visualization, and analysis platform. *Journal of cheminformatics* **2012**, *4* (1), 1-17.
(40) Kühne, T. D.; Iannuzzi, M.; Del Ben, M.; Rybkin, V. V.; Seewald, P.; Stein, F.; Laino, T.; Khaliullin, R. Z.; Schütt, O.; Schiffmann, F.; et al. CP2K: An electronic structure and molecular dynamics software package - Quickstep: Efficient and accurate electronic structure calculations. *Journal of Chemical Physics* **2020**, *152* (19). DOI: 10.1063/5.0007045.
(41) Mardirossian, N.; Pestana, L. R.; Womack, J. C.; Skylaris, C. K.; Head-Gordon, T.; Head-Gordon, M. Use of the rVV10 Nonlocal Correlation Functional in the B97M-V Density Functional: Defining B97M-rV and Related Functionals. *Journal of Physical Chemistry Letters* **2017**, *8* (1), 35-40. DOI: 10.1021/acs.jpclett.6b02527.
(42) VandeVondele, J.; Hutter, J. Gaussian basis sets for accurate calculations on molecular systems in gas and condensed phases. *Journal of Chemical Physics* **2007**, *127* (11). DOI: 10.1063/1.2770708.
(43) Lu, T.; Chen, F. W. Multiwfn: A multifunctional wavefunction analyzer. *Journal of Computational Chemistry* **2012**, *33* (5), 580-592. DOI: 10.1002/jcc.22885.
(44) Dolomanov, O. V.; Bourhis, L. J.; Gildea, R. J.; Howard, J. A. K.; Puschmann, H. OLEX2: a complete structure solution, refinement and analysis program. *Journal of Applied Crystallography* **2009**, *42*, 339-341. DOI: 10.1107/s0021889808042726.
(45) Celli, A.; Marchese, P.; Sullalti, S.; Berti, C.; Barbiroli, G. Eco-friendly Poly(butylene 1,4-cyclohexanedicarboxylate): Relationships Between Stereochemistry and Crystallization Behavior. *Macromolecular Chemistry and Physics* **2011**, *212* (14), 1524-1534. DOI: 10.1002/macp.201100052.
(46) Fraser, R. D. B.; Macrae, T. P.; Miller, A.; Rowlands, R. J. DIGITAL PROCESSING OF FIBER DIFFRACTION PATTERNS. *Journal of Applied Crystallography* **1976**, *9* (APR1), 81-94. DOI: 10.1107/s0021889876010674.

(47) Tashiro, K.; Ishino, K.; Ohta, T. Temperature dependence of crystal structure of uniaxially-oriented polyethylene analysed by an X-ray imaging plate system. *Polymer* **1999**, *40* (12), 3469-3478. DOI: 10.1016/s0032-3861(98)00553-9.
(48) Momma, K.; Izumi, F. VESTA: a three-dimensional visualization system for electronic and structural analysis. *Journal of Applied Crystallography* **2008**, *41*, 653-658. DOI: 10.1107/s0021889808012016.
(49) Zhang, C. B.; Wang, L.; Yang, B.; Zhao, H.; Liu, G. M.; Wang, D. J. Stress-induced Solid-Solid Crystal Transition in Trans-1,4-polyisoprene. *Chinese Journal of Polymer Science* **2022**, *40* (3), 256-265. DOI: 10.1007/s10118-022-2659-7.
(50) Qiu, Z. B.; Komura, M.; Ikehara, T.; Nishi, T. Miscibility and crystallization behavior of biodegradable blends of two aliphatic polyesters.: Poly(butylene succinate) and poly(ε-caprolactone). *Polymer* **2003**, *44* (25), 7749-7756. DOI: 10.1016/j.polymer.2003.10.013.
(51) Yasuniwa, M.; Tsubakihara, S.; Sugimoto, Y.; Nakafuku, C. Thermal analysis of the double-melting behavior of poly(L-lactic acid). *Journal of Polymer Science Part B-Polymer Physics* **2004**, *42* (1), 25-32, Article. DOI: 10.1002/polb.10674.
(52) Isasi, J. R.; Alamo, R. G.; Mandelkern, L. The thermal expansion of the monoclinic unit cell of isotactic polypropylene. *Journal of Polymer Science Part B-Polymer Physics* **1997**, *35* (17), 2945-2949.
(53) Shen, M.; Hansen, W. N.; Romo, P. C. THERMAL EXPANSION OF POLYETHYLENE UNIT CELL. *Journal of Chemical Physics* **1969**, *51* (1), 425-&. DOI: 10.1063/1.1671742.
(54) Skrbic, Z.; Divjakovic, V. Temperature influence on changes of parameters of the unit cell of biopolymer PHB. *Polymer* **1996**, *37* (3), 505-507. DOI: 10.1016/0032-3861(96)82922-3.
(55) Huo, P. P.; Cebe, P.; Capel, M. REAL-TIME X-RAY-SCATTERING STUDY OF THERMAL-EXPANSION OF POLY(BUTYLENE TEREPHTHALATE). *Journal of Polymer Science Part B-Polymer Physics* **1992**, *30* (13), 1459-1468, Article. DOI: 10.1002/polb.1992.090301305.
(56) Flory, P. J.; Yoon, D. Y. MOLECULAR MORPHOLOGY IN SEMI-CRYSTALLINE POLYMERS. *Nature* **1978**, *272* (5650), 226-229. DOI: 10.1038/272226a0.
(57) Men, Y. F.; Rieger, J.; Strobl, G. Role of the entangled amorphous network in tensile deformation of semicrystalline polymers. *Physical Review Letters* **2003**, *91* (9). DOI: 10.1103/PhysRevLett.91.095502.
(58) Wang, Y. T.; Jiang, Z. Y.; Wu, Z. H.; Men, Y. F. Tensile Deformation of Polybutene-1 with Stable Form I at Elevated Temperature. *Macromolecules* **2013**, *46* (2), 518-522. DOI: 10.1021/ma302389j.